

change in intensity from this value. Care was taken to omit all changes that were due to focal shifts or sample movement in any dimension. The spatial extent (half-maximal width) of local flashes was measured from line scans of $\Delta F/F_0$ at the time of maximal intensity change. To determine the effects of the pharmacological agents, we followed and compared the summed length of the same processes in control Ringer's solution and after applying the agents. Because the distribution of neuronal processes is largely two-dimensional in the retina, complete representations of the majority of dendrites could be obtained in single planes. Comparison of the total length of the processes in control solution at two time points, 20 min apart, indicated that addition and retraction of processes were balanced, with no net change in total length²⁵. The total length was then measured 25–30 min after the drug was introduced. Changes in total length upon drug treatment were expressed as a percentage of baseline length. The rate of change was calculated by dividing this number by the time between measurements (% change per min). In the uncaging experiments, we measured the total length of all terminal processes in focus that were at least partially located within 20 μm around the centre of the laser spot, before and after stimulation. All other terminal dendrites outside this region of maximal stimulation served as controls. The average initial lengths of individual terminal dendrites were similar for both groups (inside and outside the stimulated area). All statistical analyses: *t*-test, paired or unpaired.

Received 23 March; accepted 1 May 2002; doi:10.1038/nature00850.

- Yuste, R. & Tank, D. W. Dendritic integration in mammalian neurons, a century after Cajal. *Neuron* **16**, 701–703 (1996).
- Cline, H. T. Dendritar arbor development and synaptogenesis. *Curr. Opin. Neurobiol.* **11**, 118–126 (2001).
- Wong, W. T. & Wong, R. O. L. Rapid dendritic movements during synapse formation and rearrangement. *Curr. Opin. Neurobiol.* **10**, 118–124 (2000).
- Li, Z., Van Aelst, L. & Cline, H. T. Rho GTPases regulate distinct aspects of dendritic arbor growth in *Xenopus* central neurons *in vivo*. *Nature Neurosci.* **3**, 217–225 (2000).
- Wong, W. T., Faulkner-Jones, B. E., Sanes, J. R. & Wong, R. O. L. Rapid dendritic remodeling in the developing retina: dependence on neurotransmission and reciprocal regulation by Rac and Rho. *J. Neurosci.* **20**, 5024–5036 (2000).
- Wong, W. T. & Wong, R. O. L. Changing specificity of neurotransmitter regulation of rapid dendritic remodeling during synaptogenesis. *Nature Neurosci.* **4**, 351–352 (2001).
- Kettunen, P. *et al.* Rapid loading of calcium indicators by particle mediated ballistic delivery. *J. Neurosci. Methods*, in the press.
- Catsicas, M., Bonness, V., Becker, D. & Mobbs, P. Spontaneous Ca^{2+} transients and their transmission in the developing chick retina. *Curr. Biol.* **8**, 283–286 (1998).
- Sernagor, E., Eglen, S. J. & O'Donovan, M. J. Differential effects of acetylcholine and glutamate blockade on the spatiotemporal dynamics of retinal waves. *J. Neurosci.* **20**, RC56 (2000).
- Wong, W. T., Sanes, J. R. & Wong, R. O. L. Developmentally regulated spontaneous activity in the embryonic chick retina. *J. Neurosci.* **18**, 8839–8852 (1998).
- Hughes, W. F. & LaVelle, A. On the synaptogenic sequence in the chick retina. *Anat. Rec.* **179**, 297–302 (1974).
- Hering, H. & Kröger, S. Formation of synaptic specializations in the inner plexiform layer of the developing chick retina. *J. Comp. Neurol.* **375**, 393–405 (1996).
- Millar, T. J. *et al.* Cholinergic amacrine cells of the chicken retina: a light and electron microscope immunocytochemical study. *Neuroscience* **21**, 725–743 (1987).
- Wong, R. O. L., Herrmann, K. & Shatz, C. J. Remodeling of retinal ganglion cell dendrites in the absence of action potential activity. *J. Neurobiol.* **22**, 685–697 (1991).
- Berridge, M. J. Neuronal calcium signalling. *Neuron* **21**, 13–26 (1998).
- Spitzer, N. C., Lautermilch, N. J., Smith, R. D. & Gomez, T. M. Coding of neuronal differentiation by calcium transients. *Bioessays* **22**, 811–817 (2000).
- Chang, K. T. & Berg, D. K. Voltage-gated channels block nicotinic regulation of CREB phosphorylation and gene expression in neurons. *Neuron* **32**, 855–865 (2001).
- Koizumi, S. *et al.* Characterization of elementary Ca^{2+} release signals in NGF-differentiated PC12 cells and hippocampal neurons. *Neuron* **22**, 125–137 (1999).
- Korkotian, E. & Segal, M. Release of calcium from stores alters the morphology of dendritic spines in cultured hippocampal neurons. *Proc. Natl. Acad. Sci. USA* **96**, 12068–12072 (1999).
- Svoboda, K. & Mainen, Z. F. Synaptic [Ca^{2+}]: intracellular stores spill their guts. *Neuron* **22**, 427–430 (1999).
- Rose, C. R. & Konnerth, A. Stores not just for storage. Intracellular calcium release and synaptic plasticity. *Neuron* **31**, 519–522 (2001).
- Yuste, R., Majewska, A. & Holthoff, K. From form to function: calcium compartmentalization in dendrite spines. *Nature Neurosci.* **3**, 653–659 (2000).
- Eilers, J., Augustine, G. J. & Konnerth, A. Subthreshold synaptic Ca^{2+} signalling in fine dendrites and spines of cerebellar Purkinje neurons. *Nature* **373**, 155–158 (1995).
- Nishiyama, M., Hong, K., Mikoshiba, K., Poo, M. M. & Kato, K. Calcium stores regulate the polarity and input specificity of synaptic modification. *Nature* **408**, 584–588 (2000).
- Vaughn, J. E. Fine structure of synaptogenesis in the vertebrate central nervous system. *Synapse* **3**, 255–285 (1989).
- McAllister, A. K. Cellular and molecular mechanisms of dendrite growth. *Cereb. Cortex* **10**, 963–973 (2000).
- Gan, W. B., Grutzendler, J., Wong, W. T., Wong, R. O. L. & Lichtman, J. W. Multicolor "DiOlistic" labeling of the nervous system using lipophilic dye combinations. *Neuron* **27**, 219–225 (2000).
- Myhr, K. L., Lukasiewicz, P. D. & Wong, R. O. L. Mechanisms underlying developmental changes in the firing patterns of ON and OFF retinal ganglion cells during refinement of their central projections. *J. Neurosci.* **21**, 8664–8671 (2001).

Supplementary Information accompanies the paper on *Nature's* website (<http://www.nature.com/nature>).

Acknowledgements

We thank J. Sanes, J. Lichtman, A. M. Craig and S. Eglen for comments on the manuscript,

and J. Demas for assistance with ballistic loading of calcium indicators. This work was supported by NIH, NSF, DFG and the Plum foundation.

Competing interests statement

The authors declare that they have no competing financial interests.

Correspondence and requests for materials should be addressed to R.O.L.W. (e-mail: wongr@pcg.wustl.edu).

TRPV3 is a calcium-permeable temperature-sensitive cation channel

Haoxing Xu*, **I. Scott Ramsey***, **Suhas A. Kotetcha***, **Magdalene M. Moran‡**, **Jayhong A. Chong***, **Deborah Lawson§**, **Pei Ge§**, **Jeremiah Lilly§**, **Inmaculada Silos-Santiago§**, **Yu Xie§**, **Peter S. DiStefano§||**, **Rory Curtis§||** & **David E. Clapham***

* Howard Hughes Medical Institute, Children's Hospital, Harvard Medical School, Enders 1309, 320 Longwood Avenue, Boston, Massachusetts 02115, USA

‡ Program in Neuroscience, Harvard Medical School, Goldenson Building B2-228, 220 Longwood Avenue, Boston, Massachusetts 02115, USA

§ Millennium Pharmaceuticals Inc., 75 Sidney Street, Cambridge, Massachusetts 02139, USA

† These authors contributed equally to this work

Transient receptor potential (TRP) proteins are cation-selective channels that function in processes as diverse as sensation and vasoregulation. Mammalian TRP channels that are gated by heat and capsaicin (>43 °C; TRPV1 (ref. 1)), noxious heat (>52 °C; TRPV2 (ref. 2)), and cooling (<22 °C; TRPM8 (refs 3, 4)) have been cloned; however, little is known about the molecular determinants of temperature sensing in the range between ~22 °C and 40 °C. Here we have identified a member of the vanilloid channel family, human TRPV3 (hTRPV3) that is expressed in skin, tongue, dorsal root ganglion, trigeminal ganglion, spinal cord and brain. Increasing temperature from 22 °C to 40 °C in mammalian cells transfected with hTRPV3 elevated intracellular calcium by activating a nonselective cationic conductance. As in published recordings from sensory neurons, the current was steeply dependent on temperature, sensitized with repeated heating, and displayed a marked hysteresis on heating and cooling^{5–10}. On the basis of these properties, we propose that hTRPV3 is thermosensitive in the physiological range of temperatures between TRPM8 and TRPV1.

Survival depends on the precise regulation of body temperature¹¹. Certain dorsal root ganglia (DRG) neurons detect temperature changes between 32 °C and 43 °C (warmth)⁵ and respond with calcium influx processes⁷. Recordings of a nonselective ion channel activated by temperatures from 25 °C to 49 °C (ref. 6), as well as temperature-activated cationic currents in both central and sensory neurons^{8–10} are indicative of an involvement of TRP ion channels. Activation of TRP channels depolarizes cells from the resting membrane potential and shortens action potential duration. Most TRP channels are cation-nonspecific and permeant to the signal transduction element Ca^{2+} . Although all channels and enzymes are inherently temperature-sensitive, the discovery of 'hot' pepper¹, noxious heat⁸ and menthol-sensitive^{3,4} TRP channels with high 10-degree temperature coefficients (Q_{10} values (ref. 12)) motivates the search for other ion channels in the mammalian TRP superfamily.

|| Present address: Elixir Pharmaceuticals Inc. 1000, One Kendall Square, Cambridge Massachusetts 02139, USA.

Database searches revealed TRP-related expressed sequence tags (ESTs) in a human testis library. The corresponding genomic sequences were identified on human chromosome 17 near the TRPV1 locus (chromosome location 17p13). A combination of exon-prediction software, polymerase chain reaction (PCR), rapid amplification of cloned ends (RACE) and screening of a human brain complementary DNA library yielded a putative open reading frame (ORF) of 790 amino acids with homology to members of the TRPV family (Fig. 1a). The hTRPV3 cDNA is 38%, 38%, 32% and 12% identical to that of TRPV4, TRPV1, TRPV2 and TRPM8, respectively. Hidden Markov modelling¹³ of the transmembrane topology of the amino acid sequence of hTRPV3 was consistent with a primary structure containing six transmembrane domains (Fig. 1b). As is characteristic for other TRPV and TRPC family channels (Fig. 1c), hTRPV3 contains three putative ankyrin repeats (Fig. 1a).

TaqMan quantitative PCR with reverse transcription (RT-PCR) of 22 different human tissues revealed high TRPV3 expression in brain, spinal cord, DRG, skin and testis. Lower expression was seen in stomach, trachea, small intestine and placenta (see Supplementary Information). Expression of an approximately 5-kilobase (kb) transcript in tongue and stomach was also detected by northern blot analysis (see Supplementary Information). *In situ* hybridization of monkey tissue with an antisense RNA probe derived from the 3' end

of the coding region of TRPV3 labelled neurons throughout the cortex, thalamus and striatum (Fig. 2; see also Supplementary Information). In the spinal cord, TRPV3 was present in ventral horn motoneurons, as well as interneurons in the intermediate zone and deep laminae of the dorsal horn, but not in the superficial dorsal horn (laminae I and II). In the peripheral nervous system, TRPV3 was detected in sympathetic neurons in the superior cervical ganglia (SCG) and in most of the sensory neurons in the DRG and trigeminal ganglia (Fig. 2). Bright field microscopy revealed that TRPV3 RNA is present in DRG sensory neurons of all sizes, including the small nociceptive neurons that previously were shown to express the heat-sensitive channel TRPV1 and the cold-sensor channel TRPM8 (refs 1, 3, 4, 14). No signal was detected in glial cells in either the central or peripheral nervous system. Finally, TRPV3 was detected in the upper layer of monkey tongue (data not shown) and in cells surrounding hair follicles of human skin that receive sensory and sympathetic innervation¹⁵.

Given the homology of hTRPV3 to other heat-activated channels, we tested whether hTRPV3 coded for a functional heat-sensitive and Ca^{2+} -permeable channel. One defining characteristic for temperature-gated channels is a rapid, nonlinear change as a functional response to temperature changes. We transfected hTRPV3 into CHO-K1 (Chinese hamster ovary) cells and measured intracellular calcium ($[\text{Ca}^{2+}]_i$) concentration responses and hTRPV3 currents

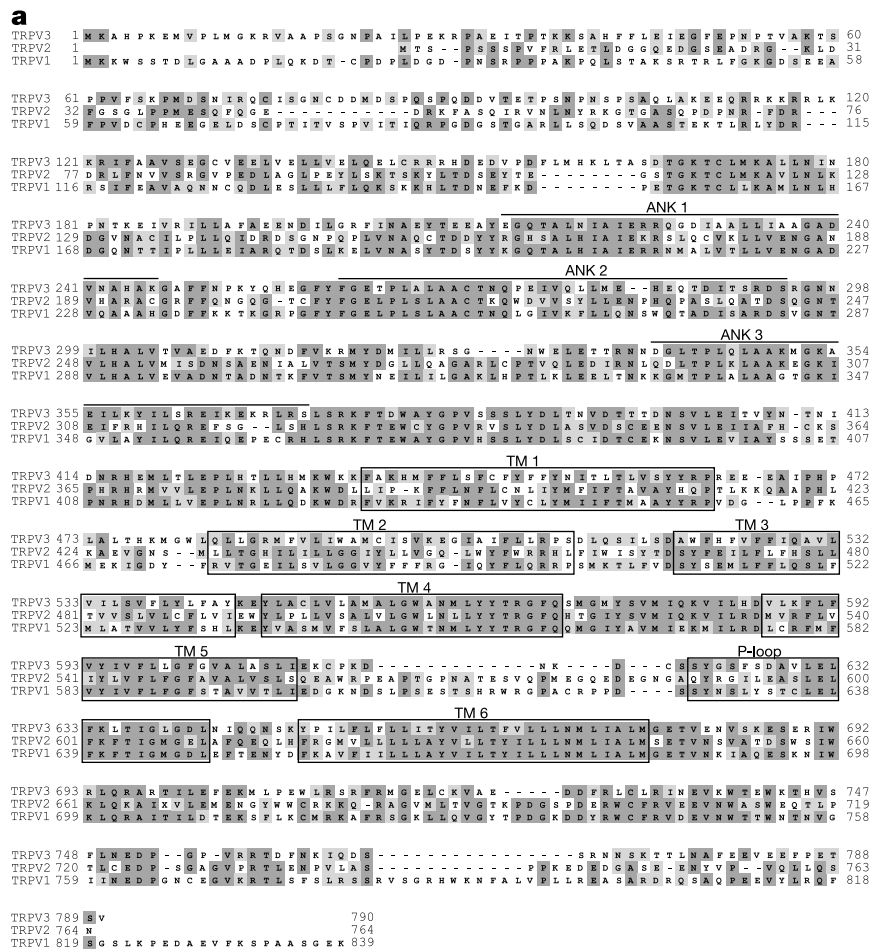


Figure 1 Deducing primary amino acid sequence of hTRPV3 and alignment with hTRPV1 and hTRPV2. **a**, The putative six transmembrane domains (TM 1–6), pore region, and 3 amino-terminal ankyrin repeats are indicated. The carboxy terminus contains a TRP family sequence (WRLQR) and a consensus PDZ binding motif, ETSV. Identical and homologous residues are shaded in dark and light grey, respectively. GenBank accession numbers for

sequences used in the alignment are NP_542437 (hTRPV1), NP_057197 (hTRPV2) and AF514998 (hTRPV3). **b**, Hidden Markov modelling predicts six transmembrane domains (1–6) and a pore region (P). **c**, Phylogenetic tree of the TRP ion channel superfamily. PAM is defined as ‘point accepted mutation’ in the MacVector software, Oxford Molecular Group.

(I_{hTRPV3}) 24 h later. Cells were loaded with the Ca^{2+} -sensitive fluorescent dye Fura-2 AM, and fluorescence ratios recorded during perfusion of a heated bath solution. Vector-transfected CHO-K1 cells exhibited no appreciable increase in $[\text{Ca}^{2+}]_i$ in response to a temperature ramp. In contrast, $[\text{Ca}^{2+}]_i$ in cells transfected with hTRPV3 exhibited an average peak increase of $398 \pm 94 \text{ nM}$ (mean \pm s.e.m.) in response to a temperature ramp from 22°C to 38°C over 12–15 s ($n = 34$ cells, Fig. 3a, b). The response decayed slowly when the temperature was maintained at a plateau temperature. Reduction of extracellular calcium to nominal concentrations ($\sim 10 \mu\text{M}$) reduced $[\text{Ca}^{2+}]_i$ to basal levels ($60 \pm 20 \text{ nM}$; Fig. 3a, $n = 26$ cells).

Increasing bath temperature from 23°C to 36°C (initial rate = 0.7°C s^{-1}) elicited a large outwardly rectifying whole-cell current (I_{hTRPV3} , Fig. 3c–f). I_{hTRPV3} readily activated above room temperature ($22.6 \pm 0.1^\circ\text{C}$) and rapidly deactivated after removal

of the heating stimulus (Fig. 3c). The average heat-activated I_{hTRPV3} was $1.4 \pm 0.3 \text{ nA}$ at $+80 \text{ mV}$ and $-0.42 \pm 0.12 \text{ nA}$ at -80 mV (mean \pm s.e.m.). We frequently observed that a residual component of I_{hTRPV3} decayed slowly after cooling from peak temperatures (Fig. 3c, d). Similar heating protocols applied to vector- and non-transfected cells failed to activate a similar current (Fig. 3c). I_{hTRPV3} reversed near 0 mV (Fig. 3d), as expected for nonselective cation channels. Large, fast-current fluctuations about the mean I_{hTRPV3} were observed at both negative and positive membrane potentials (Fig. 3c, d), a characteristic of neuronal heat-activated currents⁸.

No currents were measured in cells transfected with hTRPV3 when agonists of TRPV1 (10 μM capsaicin, 10 μM resiniferatoxin, pH 4.3) or TRPV2 (10 nM insulin-like growth factor-I)¹⁶ were applied at 22°C . Activators of TRPV4 (hypotonic solution 250 mosM^{17,18} and 10 μM phorbol ester (PDD¹⁹) also failed to

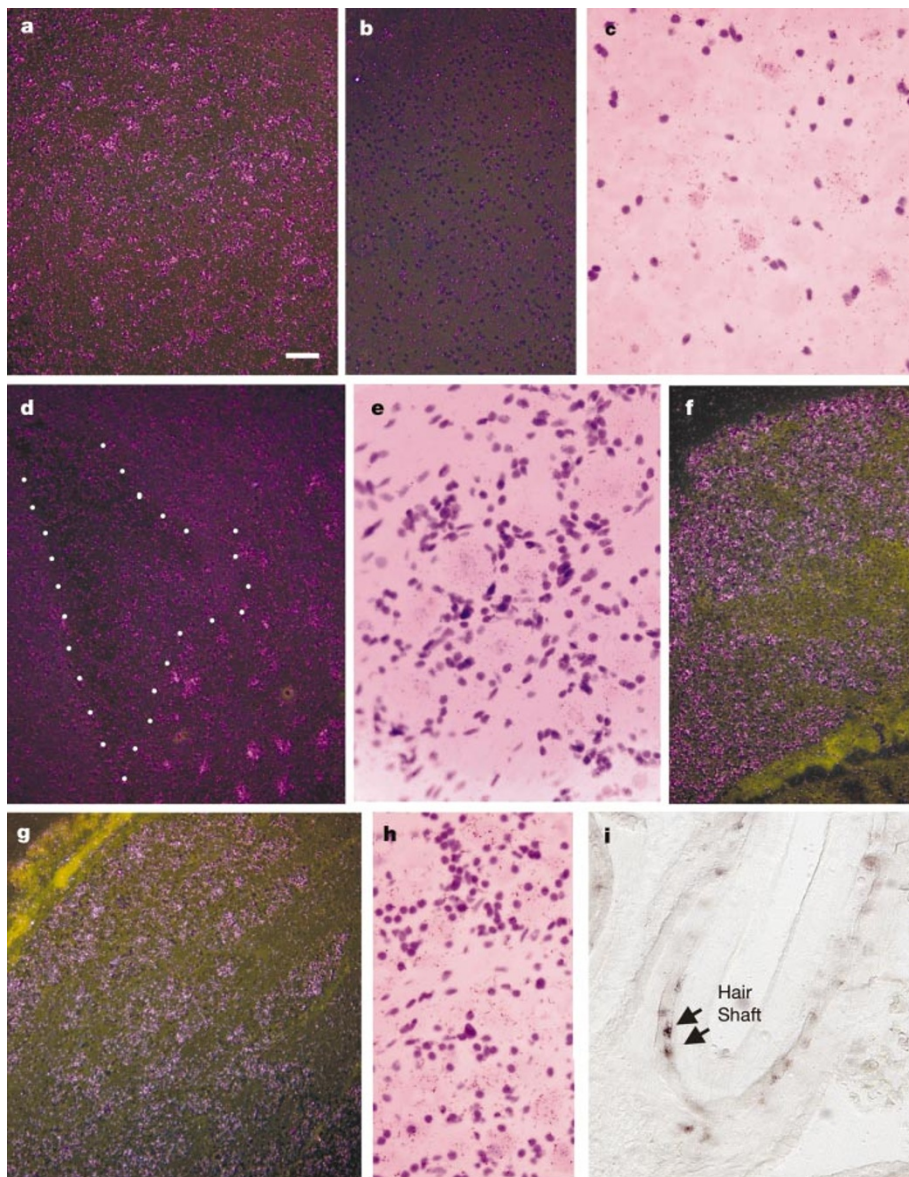


Figure 2 *In situ* hybridization of monkey tissue sections showing expression of TRPV3 in central and peripheral neurons and in the skin. **a–i**, Emulsion autoradiograms of monkey cortex (**a**), cortex sense probe control (**b**), thalamus (**c**), dorsal spinal cord (**d**), trigeminal ganglion (**e**), superior cervical ganglion (**f**), dorsal root ganglion (**g**, **h**), and human hair

follicle root sheath cells (arrows) (**i**). Note the lack of expression in the superficial laminae of the dorsal horn (dotted line in **d**). Scale bar: 40 μm for $\times 10$ magnification dark field images (**a**, **b**, **d**, **f**, **g**); 10 μm for $\times 40$ magnification bright field images (**c**, **e**, **h**, **i**).

activate any new currents in hTRPV3-transfected cells at 22 °C. To exclude contamination by native Mg²⁺-inhibited current^{20–22}, we commonly studied the temperature-dependent activation of $I_{h\text{TRPV}3}$ in the presence of 10 mM [Mg²⁺]_i.

$I_{h\text{TRPV}3}$ was cation-nonspecific (Fig. 3e) with relative permeabilities of Ca²⁺ > Na⁺ ≈ K⁺ ≈ Cs⁺ and permeability ratios as listed in Fig. 3f. Ruthenium red (10 μM), a nonselective blocker of many cation channels, blocked heat-evoked $I_{h\text{TRPV}3}$ by 89 ± 3% (holding potential, V_h = -40 mV, n = 5, P < 0.05). In contrast, the TRPV1 antagonist capsazepine (10 μM) failed to significantly block the current (5.2 ± 2% at V_h = +60 mV, n = 4). The failure of capsaicin to activate and capsazepine to block $I_{h\text{TRPV}3}$ agrees with the predicted absence of a capsaicin-binding site²³ in the hTRPV3 sequence.

$I_{h\text{TRPV}3}$ activates rapidly in response to voltage steps with no evidence of time-dependent inactivation (Fig. 4a, b). Outside-out, single-channel recordings from hTRPV3-expressing cells revealed that the single channel current–voltage (I–V) relation was outwardly rectifying with a chord conductance of 172 ± 9 pS at +60 mV (n = 4; Fig. 4c). At +60 mV, the single-channel mean open time was 5.4 ± 0.2 ms (n = 4; Fig. 4d). Consistent with the behaviour of the whole-cell current, single-channel opening probability increased markedly with temperature elevation from 25 °C to

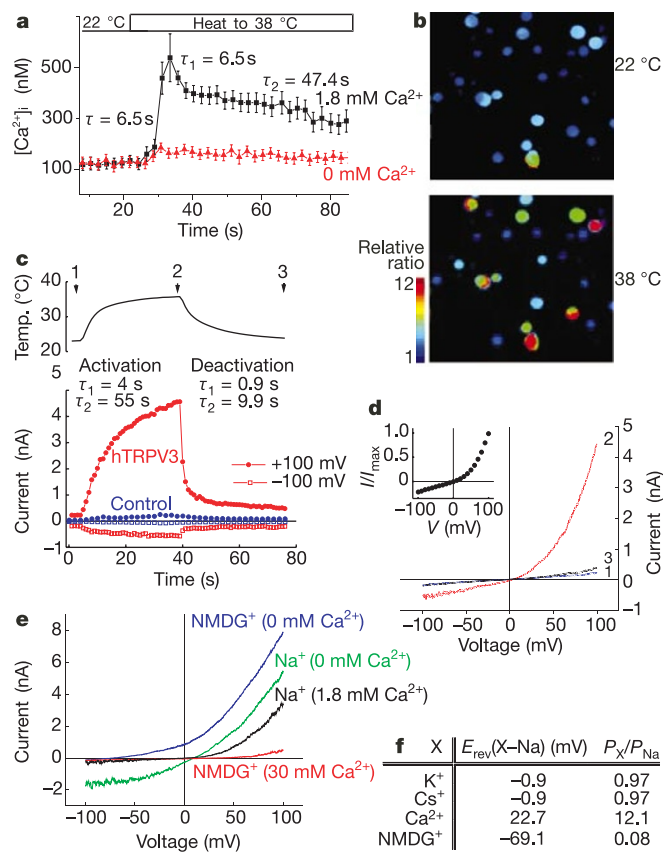


Figure 3 Temperature-activated currents and [Ca²⁺]_i increases in hTRPV3-expressing CHO-K1 cells. **a**, Fura-2-measured changes of [Ca²⁺]_i with changing temperature. **b**, Heat-induced Ca²⁺ response in CHO-K1 cells. **c**, Activation of $I_{\text{TRPV}3}$ by temperature elevation. Representative whole-cell currents at +100 mV or -100 mV in CHO-K1 cells transfected with hTRPV3 or pTracer vector. **d**, hTRPV3 I–V relation determined from voltage ramps (-100 to +100 mV, 200 ms). Numbers correspond to the time course in **c**. The inset shows normalized $I_{\text{hTRPV}3}$ (mean ± s.e.m., n = 18). **e**, $I_{\text{hTRPV}3}$ is carried by monovalent cations and Ca²⁺. **f**, Calculated relative permeabilities of $I_{\text{TRPV}3}$. E_{rev} is the reversal potential; τ is the time constant.

37 °C (Fig. 4e, f).

Activation of $I_{\text{hTRPV}3}$ at -60 mV is correlated with the initial rate of heating (Fig. 5a). Rapid heating (4.1–6.0 °C s⁻¹) elicited larger hTRPV3 currents (-648.3 ± 237.2 pA at 32 °C) than slower heating protocols (-158.3 ± 33.0 pA at 32 °C). One method used to quantify the temperature sensitivity of ion channels is the 10-degree temperature coefficient (Q_{10}), corresponding to the inverse slope of log (I) plotted against 1/T, where T is absolute temperature (Arrhenius plot^{12,24}; Fig. 5b). Q_{10} values for the membrane conductance of relatively ‘temperature-insensitive’ channels is approximately 1.5. In contrast, hTRPV3-transfected cells exposed to slow heating protocols usually showed an initial activation phase ($Q_{10} = 1.9 \pm 0.3$, n = 16 cells) followed by a second steep phase ($Q_{10} = 17.3 \pm 3.0$, n = 19 cells) corresponding to ~11.4 and ~54.0 kcal mol⁻¹, respectively. The slope of the second phase is unlike temperature-insensitive conductances, but comparable to data we replotted from $I_{\text{TRPV}1}$, $I_{\text{TRPV}2}$ (refs 2, 14) and I_{heat} in neurons^{10,25,26}. The inflection point of these two phases is referred to as the thermal threshold (T_h)^{8,10,26}. In cells that clearly exhibited both a first and second phase, $T_h = 31 \pm 2$ °C (n = 12) was close to the threshold for warm-sensitive neurons^{9,27} and warm-activated currents in neurons^{9,10}. Cells exposed to rapid heating typically exhibited a steep initial activation phase ($Q_{10} = 21.6 \pm 4.2$,

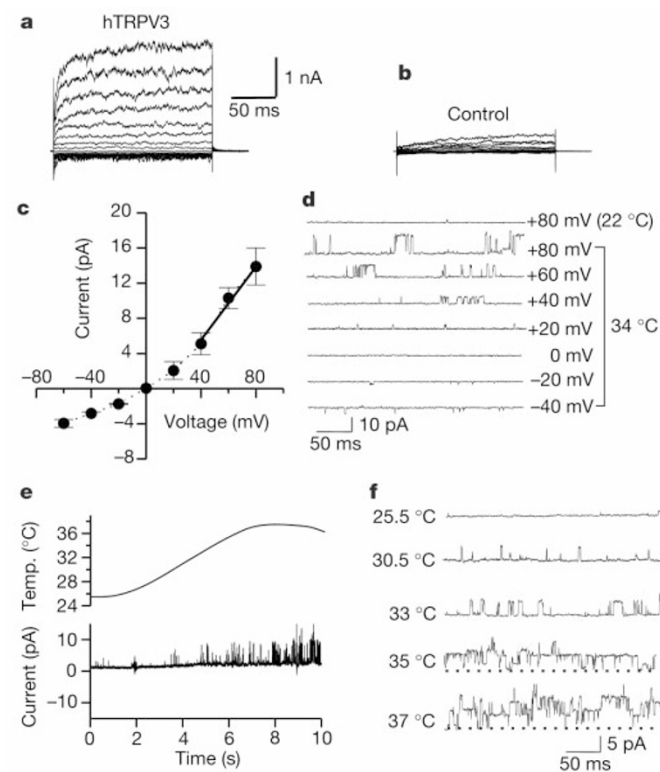


Figure 4 Temperature-activated hTRPV3 currents. **a**, **b**, Kinetics of temperature-activated whole-cell currents resulting from 200-ms voltage steps from -100 to +100 mV in 10-mV increments in CHO-K1 cells transfected with hTRPV3 (**a**) or pTracer vector (**b**). **c**, hTRPV3 single-channel I–V relation at 34 °C. A linear regression fit from +40 to +80 mV (solid line) yielded a slope conductance of 197 ± 11 pS (mean ± s.e.m., n = 4). Chord conductance was 172 ± 9 pS at +60 mV. Channel amplitudes were determined by measuring amplitude histograms at each potential. **d**, Representative single channel traces at different holding potentials. **e**, Single-channel currents (outside-out patches) of hTRPV3-transfected cells in response to a temperature ramp. Current activated most prominently at temperatures above 30 °C. **f**, Representative single-channel currents ($V_h = +60$ mV) in response to a temperature ramp from 24.5 °C to 37 °C. Dashed lines indicate the closed state.

$n = 11$) that was followed by a more shallow phase ($Q_{10} = 3.9 \pm 0.7$, $n = 14$ cells). I_{hTRPV3} did not saturate up to the highest temperature tested (50 °C). Similar variable heat responses were also recorded for the capsaicin- and pH-insensitive heat-activated current in trigeminal neurons¹⁰.

Repeated temperature elevation increased both the steady-state current and the current variance (Fig. 5c). I_{hTRPV3} was differentially sensitive to the direction of temperature change, resulting in hysteresis of the thermal activation–deactivation cycle. Whereas increasing temperature resulted in progressive activation of I_{hTRPV3} , even small decreases in temperature profoundly affected current deactivation (Fig. 5d). Loop hysteresis was independent of the absolute temperature reached during the heating protocol (Fig. 5d). Heat-induced activation of I_{hTRPV3} also accelerated the temporal kinetics and decreased the temperature-dependence of subsequent thermal activations (Fig. 5d, e). Q_{10} values for the first, second and third heat exposures in Fig. 5e were similar (18.7, 20.6 and 17.5, respectively). However, the zero current intercept decreased 3–4 °C after the initial heat exposure, indicating a change in the thermal sensitivity of I_{hTRPV3} . The hysteresis effect predicts that the immediate history of temperature activation will affect the current induced in cells expressing I_{hTRPV3} . Both the speed of

temperature change and the absolute temperature affect I_{hTRPV3} , consistent with data from primary afferent warm-sensitive fibres²⁷.

We found that I_{hTRPV3} codes for a highly temperature-sensitive ion channel uniquely sensitive around the physiological 37 °C temperature point in mammals. The temperature dependence of I_{hTRPV3} fills a gap between the cool-sensing TRPM8 (25 °C to 15 °C) and the heat-sensing TRPV1 (>43 °C) channels. In DRG neurons, not all low-threshold, heat-induced responses are sensitive to capsaicin²⁸. Identification of I_{hTRPV3} as a heat-sensitive but capsaicin-insensitive cation channel may help explain these previous findings. The apparent disparity between robust primate TRPV3 expression reported here and sparse warm-sensitive responses in rodent sensory neurons and fibres⁷ could result from inter-species variability, post-transcriptional or -translational regulation or hetero-oligomerization of TRPV3 with TRPV channels that respond only at higher temperatures. I_{hTRPV3} may report graded responses to warm stimuli in peripheral tissues that are normally below (17 °C–22 °C) the channel's thermal threshold, but responds robustly to small perturbations around core body temperature (36 °C to 38 °C). The wide tissue distribution of I_{hTRPV3} suggests that I_{hTRPV3} may have additional, as yet unidentified functions. □

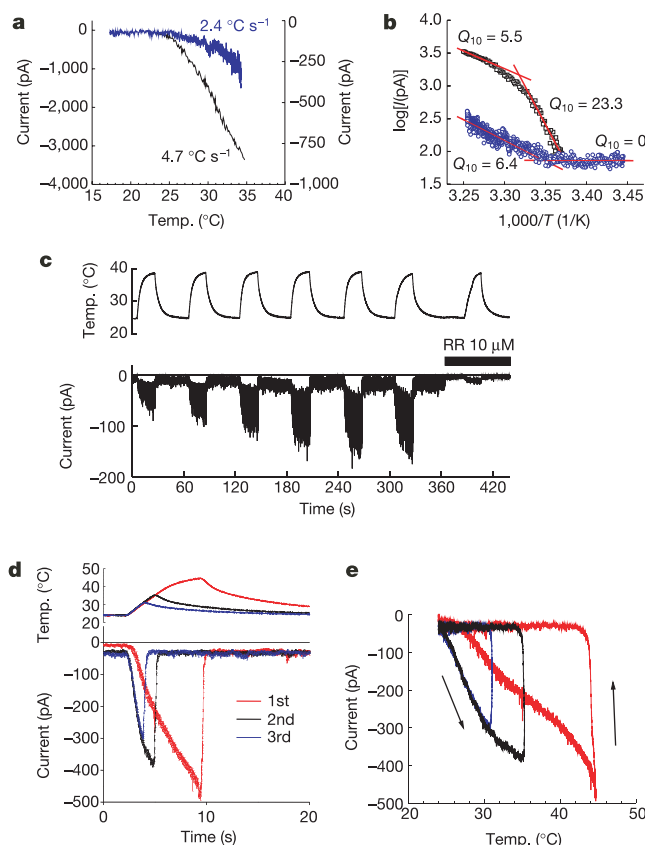


Figure 5 Temperature-dependent gating of I_{hTRPV3} . **a**, I_{hTRPV3} –temperature (T) response from two cells recorded at -60 mV at the initial heating rates indicated. Higher dT/dt (where t is time) characteristically evoked larger currents (black trace, left y axis). **b**, Arrhenius plots of the data in **a** illustrate three phases of the thermal response. Q_{10} values were derived from linear fits of the data and the plots demonstrate the range of variability. **c**, Sensitization of I_{hTRPV3} on repeated heat stimulation is characteristic of I_{hTRPV3} and is blocked by ruthenium red (RR 10 μ M). **d**, Repeated heating speeds I_{hTRPV3} activation rates without altering deactivation. **e**, Hysteresis of I_{hTRPV3} in response to heating and cooling. Arrows indicate temporal direction of current response.

Methods

Cloning

To identify new TRP channels, we searched the NCBI, Millennium EST, ENSEMBL, and Celera databases with the sequences of known TRPV channels. A full-length human I_{hTRPV3} cDNA containing a 2,373-nucleotide ORF was isolated from a human brain cDNA library using the primers 5'-GCCACGACCACCCAGAACCTCA-3' and 5'-CACCCACTGAGCACTGAGCACGAGG-3'. Both 3' and 5' RACE reactions established that this clone contained the entire ORF.

RT-PCR and *in situ* hybridization

Expression of I_{hTRPV3} in a panel of human nervous system and peripheral tissues was assessed by TaqMan real time quantitative RT-PCR (essentially as previously described²⁹) using the following primers in the 3' end of the coding region, giving an amplicon of 64 bp: sense, 5'-GAGCAGATTCCGGATGGGA-3'; antisense, 5'-CCGAAACACAGTCGGAAA-3'; fluorescent probe, 5'-CATCCTCGGCCACTTGCACAGCT-3'. β 2-microglobulin RNA was used as the internal reference for gene expression.

To determine cellular expression, 12- μ m fresh-frozen sections were prepared from cynomolgus monkey tissues (brain, DRG, spinal cord and SCG). *In situ* hybridization was performed using a 35 S-labelled, 247-bp human I_{hTRPV3} cRNA probe covering amino acids 672–754, essentially as described²⁹. A 33 P-labelled cRNA probe (~600 bp) extending from the EcoRI to the EcoRV sites in the 3' end of I_{hTRPV3} was hybridized to a multiple human tissue northern blot (MTN3, Clontech). The same probe labelled with digoxigenin was hybridized to human scalp tissue.

Mammalian cell electrophysiology

I_{hTRPV3} was subcloned into a green fluorescence protein (GFP)-containing vector (pTracer-CMV2, Invitrogen) for expression in CHO-K1 cells. Cells were transfected using LT2 polyamine (PanVera) or Lipofectamine 2000 (Invitrogen) transfection reagent (6–8 h). Transfected cells, cultured at 37 °C, were plated onto glass coverslips and recorded 24 to 48 h later. Unless otherwise stated, the pipette solution contained (in mM): 147 Cs, 120 methane-sulphonate, 8 NaCl, 10 EGTA, 2 Mg-ATP, and 20 HEPES, pH 7.4. Bath solution contained (in mM): 138 NaCl, 1.8 CaCl₂, 5 KCl, 20 HEPES, pH 7.4, and 10 glucose. Data were collected using an Axopatch 2A patch clamp amplifier, Digidata 1320, and pClamp 8.0 software. Whole-cell and excised outside-out patch currents were filtered at 2 kHz and digitized at 10 kHz. The perfuse was heated using a Warner TC-333A or TC-344B heater controller and either Warner SHM-6 or SH-27B solution heater. In some experiments, the bath solution was cooled before heating. The rate of temperature change was between 0.7 °C and 6.0 °C s⁻¹, depending on the flow rate. For determination of the current–voltage relation, background currents before heat stimuli were subtracted from responses in the presence of heat. In experiments performed with high [Mg²⁺]_i to block endogenous currents, the pipette solution contained (in mM): 145 Cs-gluconate, 10 MgCl₂, 10 Cs₄-BAPTA, 10 HEPES, pH 7.2. Heat-activated I_{hTRPV3} in high [Mg²⁺]_i was not detectably different from those recorded in standard pipette solution.

The permeability of monovalent cations relative to that of Na⁺ was estimated from the shift in reversal potential on replacing external Na⁺ in nominally Ca²⁺-free bath solution (145 mM XCl, 20 mM HEPES, 10 mM glucose, pH 7.4), where X was Na⁺, K⁺, Cs⁺, or NMDG⁺. Ca²⁺ permeability was estimated from the shift in reversal potential on replacing NMDG-Cl with solution containing (in mM): 100 NMDG-Cl, 30 CaCl₂, 20

HEPES, 10 glucose, pH 7.4 (see equation (2)³⁰).

$$P_{\text{X}}/P_{\text{Na}} = \{[\text{Na}^+]_o/[\text{X}]_o\} \{\exp((F/RT)(V_{\text{X}} - V_{\text{Na}}))\} \quad (1)$$

$$P_{\text{Ca}}/P_{\text{Na}} = \{[\text{Na}^+]_o/4[\text{Ca}^{2+}]_o\} \{\exp((F/RT)(V_{\text{Ca}} - V_{\text{Na}}))\} \{1 + \exp(FV_{\text{Ca}}/RT)\} \quad (2)$$

where $[\text{X}]_o$ is defined as the extracellular concentration of the given ion, P is defined as the permeability of the ion indicated by the subscript, F is Faraday's constant, R is the gas constant, T is absolute temperature and V is the reversal potential for the ion indicated by the subscript.

Calcium imaging

Cells were loaded with 2 μM Fura-2 AM in cell culture medium at room temperature for 30 min. We recorded Fura-2 ratios (F340/F380) on a MERLIN imaging system (Olympus). The standard curve for Fura-2 ratio versus Ca^{2+} concentration was constructed using the Fura-2 calcium imaging calibration kit (Molecular Probes).

Data analysis

Group data are presented as mean ± s.e.m. Statistical comparisons were made using analysis of variance and the *t*-test with Bonferroni correction. A two-tailed value of $P < 0.05$ was taken to be statistically significant.

Received 26 April; accepted 28 May 2002; doi:10.1038/nature00882.

Published online 23 June 2002; corrected 11 July (details online).

1. Caterina, M. J. *et al.* The capsaicin receptor: a heat-activated ion channel in the pain pathway. *Nature* **389**, 816–824 (1997).
2. Caterina, M. J., Rosen, T. A., Tominaga, M., Brake, A. J. & Julius, D. A capsaicin-receptor homologue with a high threshold for noxious heat. *Nature* **398**, 436–441 (1999).
3. McKemy, D. D., Neuhauser, W. M. & Julius, D. Identification of a cold receptor reveals a general role for TRP channels in thermosensation. *Nature* **416**, 52–58 (2002).
4. Peier, A. M. *et al.* A TRP channel that senses cold stimuli and menthol. *Cell* **108**, 705–715 (2002).
5. Spray, D. C. Cutaneous temperature receptors. *Annu. Rev. Physiol.* **48**, 625–638 (1986).
6. Reichling, D. B. & Levine, J. D. Heat transduction in rat sensory neurons by calcium-dependent activation of a cation channel. *Proc. Natl Acad. Sci. USA* **94**, 7006–7011 (1997).
7. Gotob, H., Akatsuka, H. & Suto, K. Warm cells revealed by microfluorimetry of Ca^{2+} in cultured dorsal root ganglion neurons. *Brain Res.* **796**, 319–322 (1998).
8. Cesare, P., Moriondo, A., Vellani, V. & McNaughton, P. A. Ion channels gated by heat. *Proc. Natl Acad. Sci. USA* **96**, 7658–7663 (1999).
9. Hori, A., Minato, K. & Kobayashi, S. Warming-activated channels of warm-sensitive neurons in rat hypothalamic slices. *Neurosci. Lett.* **275**, 93–96 (1999).
10. Liu, L. & Simon, S. A. Capsaicin, acid and heat-evoked currents in rat trigeminal ganglion neurons: relationship to functional VR1 receptors. *Physiol. Behav.* **69**, 363–378 (2000).
11. Brengelmann, G. L. in *Textbook of Physiology Volume 2: Circulation, Respiration, Body Fluids, Metabolism, and Endocrinology* (eds Patton, H. D., Fuchs, A. E., Hille, B., Scher, A. M. & Steiner, R.), 1584–1596, (W.B. Saunders, Philadelphia, 1989).
12. Hille, B. *Ion Channels of Excitable Membranes* (Sinauer Associates, Sunderland, Massachusetts, 2001).
13. Möller, S., Croning, M. D. & Apweiler, R. Evaluation of methods for the prediction of membrane spanning regions. *Bioinformatics* **17**, 646–653 (2001).
14. Tominaga, M. *et al.* The cloned capsaicin receptor integrates multiple pain-producing stimuli. *Neuron* **21**, 531–543 (1998).
15. Fundin, B. T., Rice, F. L., Pfaller, K. & Arvidsson, J. The innervation of the mystacial pad in the adult rat studied by anterograde transport of HRP conjugates. *Exp. Brain Res.* **99**, 233–246 (1994).
16. Kanazaki, M. *et al.* Translocation of a calcium-permeable cation channel induced by insulin-like growth factor-1. *Nature Cell. Biol.* **1**, 165–170 (1999).
17. Liedtke, W. *et al.* Vanilloid receptor-related osmotically activated channel (VR-OAC), a candidate vertebrate osmoreceptor. *Cell* **103**, 525–535 (2000).
18. Strotmann, R., Harteneck, C., Nunnenmacher, K., Schultz, G. & Plant, T. D. OTRPC4, a nonselective cation channel that confers sensitivity to extracellular osmolarity. *Nature Cell Biol.* **2**, 695–702 (2000).
19. Watanabe, H. *et al.* Activation of TRPV4 channels (hVR-2/mTRP12) by phorbol derivatives. *J. Biol. Chem.* **4**, 13569–13577 (2002).
20. Prakriya, M. & Lewis, R. S. Separation and characterization of currents through store-operated CRAC channels and Mg^{2+} -inhibited cation (MIC) channels. *J. Gen. Physiol.* **119**, 487–508 (2002).
21. Nadler, M. J. *et al.* LTRPC7 is a Mg-ATP-regulated divalent cation channel required for cell viability. *Nature* **411**, 590–595 (2001).
22. Runnels, L. W., Yue, L. & Clapham, D. E. TRP-PLIK, a bifunctional protein with kinase and ion channel activities. *Science* **291**, 1043–1047 (2001).
23. Jordt, S. E. & Julius, D. Molecular basis for species-specific sensitivity to 'hot' chili peppers. *Cell* **108**, 421–430 (2002).
24. DeCoursey, T. E. & Cherny, V. V. Temperature dependence of voltage-gated H^+ currents in human neutrophils, rat alveolar epithelial cells, and mammalian phagocytes. *J. Gen. Physiol.* **112**, 503–522 (1998).
25. Davis, J. B. *et al.* Vanilloid receptor-1 is essential for inflammatory thermal hyperalgesia. *Nature* **405**, 183–187 (2000).
26. Vykylicky, L. *et al.* Temperature coefficient of membrane currents induced by noxious heat in sensory neurones in the rat. *J. Physiol.* **517**, 181–192 (1999).
27. Andrew, D. & Craig, A. D. Spinothalamic lamina I neurones selectively responsive to cutaneous warming in cats. *J. Physiol.* **537**, 489–495 (2001).
28. Nagy, I. & Rang, H. P. Similarities and differences between the responses of rat sensory neurons to noxious heat and capsaicin. *J. Neurosci.* **19**, 10647–10655 (1999).
29. Qu, Y. *et al.* Differential modulation of sodium channel gating and persistent sodium currents by the $\beta 1$, $\beta 2$, and $\beta 3$ subunits. *Mol. Cell Neurosci.* **18**, 570–580 (2001).
30. Lewis, C. A. Ion-concentration dependence of the reversal potential and the single channel conductance of ion channels at the frog neuromuscular junction. *J. Physiol.* **286**, 417–445 (1979).

Supplementary Information accompanies the paper on *Nature's* website (<http://www.nature.com/nature>).

Acknowledgements

We thank U. Berger, L. Yue, X. Wei, W. Yu, A. Kabakov, L. Runnels, J. Pulido, W. Cao and H. Ferriera for assistance. We are grateful to S. Glucksman, O. Tayber, L. DeFelice and members of Clapham laboratory for discussion and comments.

Competing interests statement

The authors declare competing financial interests: details accompany the paper on *Nature's* website (<http://www.nature.com/nature>).

Correspondence and requests for materials should be addressed to D.E.C. (e-mail: dclapham@enders.tch.harvard.edu). Sequences have been deposited in GenBank under accession number AF514998 (hTRPV3).

TRPV3 is a temperature-sensitive vanilloid receptor-like protein

G. D. Smith*,†, M. J. Gunthorpe*†, R. E. Kelsell‡, P. D. Hayes‡, P. Reilly*, P. Facer§, J. E. Wright*, J. C. Jerman||, J.-P. Walhin‡, L. Ooi*, J. Egerton*, K. J. Charles*, D. Smart*, A. D. Randall*, P. Anand§ & J. B. Davis*

*Neurology-CEDD, ‡Genetics Research, and ||Discovery Research, GlaxoSmithKline, Third Avenue, Harlow CM19 5AW, UK

§Peripheral Neuropathy Unit, Imperial College, Hammersmith Hospital, Du Cane Rd, London W12 0NN, UK

†These authors contributed equally to this work

Vanilloid receptor-1 (VR1, also known as TRPV1) is a thermo-sensitive, nonselective cation channel that is expressed by capsaicin-sensitive sensory afferents and is activated by noxious heat, acidic pH and the alkaloid irritant capsaicin¹. Although VR1 gene disruption results in a loss of capsaicin responses, it has minimal effects on thermal nociception^{2,3}. This and other experiments—such as those showing the existence of capsaicin-insensitive heat sensors in sensory neurons⁴—suggest the existence of thermosensitive receptors distinct from VR1. Here we identify a member of the vanilloid receptor/TRP gene family, vanilloid receptor-like protein 3 (VRL3, also known as TRPV3), which is heat-sensitive but capsaicin-insensitive. VRL3 is coded for by a 2,370-base-pair open reading frame, transcribed from a gene adjacent to VR1, and is structurally homologous to VR1. VRL3 responds to noxious heat with a threshold of about 39 °C and is co-expressed in dorsal root ganglion neurons with VR1. Furthermore, when heterologously expressed, VRL3 is able to associate with VR1 and may modulate its responses. Hence, not only is VRL3 a thermosensitive ion channel but it may represent an additional vanilloid receptor subunit involved in the formation of heteromeric vanilloid receptor channels.

On the basis of the reasoning that a family of thermoreceptors homologous to VR1 might exist, we searched public nucleotide databases for sequences homologous to those of vanilloid receptor family members. Because we had previously noted that two members of this family, TRPV6/CaT1 (ref. 5) and TRPV5/ECAC1 (ref. 6), were co-localized on chromosome 7 (ref. 7), we focused our searches in genomic regions flanking TRPV1/VR1 17p13 (ref. 8) and TRPV4/VRL-2 12q23-24.1 (ref. 9). Sequence searches of the GenBank database led to the identification of an unfinished human genomic sequence (AC025125) sharing homology with human VR1 (AJ277028). Polymerase chain reaction (PCR) and rapid amplification of complementary DNA ends (RACE) analyses were used to extend the partial gene prediction. Analysis of the sequences